Evolving Atmospheric Ion Escape from Kepler-1649 b and c: Power-Law Trends in Atmospheric Loss

Haitao Li [ID],[1,2,3,*] Xinke Wang [ID],[1,3,*] Chuanfei Dong [ID],[4] Lianghai Xie [ID],[5] Xinyi He [ID],[1,3]
Hong-Liang Yan [ID],[6,7,8] Jinxiao Qin [ID],[9,10] Nathan Mayne [ID],[2] Mei Ting Mak [ID],[2] Nikolaos Georgakarakos [ID],[11,12]
Duncan Christie [ID],[13] Yajun Zhu,[5,3] Zhaojin Rong [ID],[14,15,16] Jinlian Ma [ID],[1,3] Shi Chen,[1,3] and Hai Zhou[1,3]

[1]*National Space Science Center, Chinese Academy of Sciences, Beijing 100190, China*
[2]*Department of Physics and Astronomy, Faculty of Environment Science and Economy, University of Exeter, EX4 4QL, UK*
[3]*University of Chinese Academy of Sciences, Beijing 100049, China*
[4]*Department of Astronomy, Boston University, Boston, MA 02215, USA*
[5]*State Key Laboratory of Solar Activity and Space Weather, National Space Science Center, Chinese Academy of Sciences, Beijing 100190, China*
[6]*CAS Key Laboratory of Optical Astronomy, National Astronomical Observatories, Beijing 100101, China*
[7]*Institute for Frontiers in Astronomy and Astrophysics, Beijing Normal University, Beijing 102206, China*
[8]*School of Astronomy and Space Science, University of Chinese Academy of Sciences, Beijing 100049, China*
[9]*Department of Physics, Hebei Normal University, Shijiazhuang 050024, China*
[10]*Guo Shoujing Institute for Astronomy, Hebei Normal University, Shijiazhuang 050024, China*
[11]*Division of Science, New York University Abu Dhabi, PO Box 129188, Abu Dhabi, UAE*
[12]*Center for Astrophysics and Space Science (CASS), New York University, Abu Dhabi, PO Box 129188, Abu Dhabi, UAE*
[13]*Max-Planck-Institut für Astronomie, Königstuhl 17, 69117 Heidelberg, Germany*
[14]*Key Laboratory of Earth and Planetary Physics, Institute of Geology and Geophysics, Chinese Academy of Sciences, Beijing 100029, China*
[15]*College of Earth and Planetary Sciences, University of Chinese Academy of Sciences, Beijing 100049, China*
[16]*Mohe Observatory of Geophysics, Institute of Geology and Geophysics, Chinese Academy of Sciences, Mohe Heilongjiang 165303, China*

ABSTRACT

Rocky planets orbiting M-dwarf stars are prime targets for characterizing terrestrial atmospheres, yet their long-term evolution under intense stellar winds and high-energy radiation remains poorly understood. The Kepler-1649 system, which hosts two terrestrial exoplanets orbiting an M5V star, presents a valuable opportunity to explore atmospheric evolution in the extreme environments characteristic of M-dwarf stellar systems. In this Letter we show that both planets could have retained atmospheres over gigayear timescales. Using a multi-species magnetohydrodynamic model, we simulate atmospheric ion escape driven by stellar winds and extreme ultraviolet radiation from 0.7 to 4.8 Gyrs. The results show that total ion escape rates follow a power-law decline ($\propto \tau^{-1.6}$ for Kepler-1649 b, $\propto \tau^{-1.5}$ for Kepler-1649 c), with O^+ dominating atmospheric loss (76.8%–98.7%). The escape rates at 4.8 Gyrs are two orders of magnitude lower than those during the early epochs (1.9×10^{27} s^{-1} at 0.7 Gyr vs. 3.0×10^{25} s^{-1} at 4.8 Gyrs for planet b), while planet b consistently exhibits 1.1–1.9× higher O^+ escape rates than planet c due to its closer orbit (0.051 AU vs. 0.088 AU). Despite substantial early atmospheric erosion, both planets may still retain significant atmospheres, suggesting the potential for long-term habitability. These findings offer predictive insight into atmospheric retention in M-dwarf systems and inform future JWST observations aimed at refining habitability assessments.

Keywords: Astrobiology (74); Magnetohydrodynamical simulations (1966); Habitable planets (695); Exoplanet atmospheres (487); Stellar winds (1636)

1. INTRODUCTION

Corresponding author: Haitao Li, Lianghai Xie

lihaitao@nssc.ac.cn, h.li6@exeter.ac.uk, xielianghai@nssc.ac.cn

* Co-first authors

The search for habitable exoplanets has evolved significantly in recent decades, driven by advances in observational technology and numerical modeling (Seager 2013; Kaltenegger 2017; Barstow et al. 2022). Initially focused on broad surveys of planetary systems, the focus has shifted toward characterizing terrestrial exoplanets within the habitable zone (HZ, the region around a

star where liquid water might persist on the surface of rocky planets Gonzalez 2005; Hall et al. 2023). The importance of this endeavor lies in its potential to identify environments capable of supporting life, a question that has become increasingly urgent with the discovery of thousands of exoplanets (Schwieterman et al. 2018; Catling et al. 2018; Zhu & Dong 2021). Current research frontiers emphasize atmospheric retention and evolution, particularly for rocky planets orbiting M-dwarfs, where stellar activity poses unique challenges to habitability (Shields et al. 2016; Airapetian et al. 2020; Modi et al. 2023; Krissansen-Totton 2023).

The retention of the atmospheres of terrestrial exoplanets orbiting M-dwarfs remains a pivotal element in assessing their potential habitability (Owen & Mohanty 2016; Wordsworth & Kreidberg 2022; Kar et al. 2024). Although the HZ defines regions where liquid water could theoretically exist (Gonzalez 2005), the sustainability of an atmosphere, particularly under prolonged stellar activity, ultimately determines whether surface conditions remain biologically viable (Cockell et al. 2016; Estrela et al. 2020; Ridgway et al. 2023). For M-dwarf systems, where intense stellar winds and extreme ultraviolet (EUV) fluxes persist over gigayear timescales (Stevenson 2003; Linsky 2019; Khodachenko et al. 2021; Engle 2024), atmospheric erosion and evolution require time-dependent analysis to evaluate long-term planetary habitability (Lammer et al. 2008).

Significant progress in understanding atmospheric escape has been made through studies of exoplanetary systems (Owen 2019; Ballabio & Owen 2025). Atmospheric escape processes exhibit complex dependencies on stellar and planetary parameters that remain inadequately characterized for Earth-sized exoplanets (Gronoff et al. 2020; Luo et al. 2023). Studies of solar system analogs such as Mars reveal orders-of-magnitude variations in atmospheric ion loss over evolutionary timescales (Dong et al. 2018; Jakosky et al. 2018), while three-dimensional magnetohydrodynamic (MHD) simulations of exoplanets highlight the critical roles of varying stellar wind (Garraffo et al. 2016; Dong et al. 2017), planetary magnetic fields (Garcia-Sage et al. 2017; Peña-Moñino et al. 2024), planetary body size (Chin et al. 2024), planetary atmospheric composition (Dong et al. 2020; Lee et al. 2021), and orbital architecture (Bourrier et al. 2018; Dong et al. 2019). Recent JWST observations further underscore the importance of characterizing the atmospheres of terrestrial exoplanets and quantifying their evolutionary pathways (Santos et al. 2023; Rackham et al. 2023; TRAPPIST-1 JWST Community Initiative et al. 2024), particularly in systems where stellar activity drives non-thermal atmospheric escape.

The Kepler-1649 system provides a unique laboratory for investigating these processes, hosting two terrestrial planets at different orbital distances. Kepler-1649 b (Venus-like, 0.051 AU) and c (Earth-like, 0.088 AU) (Vanderburg et al. 2020; Coughlin 2020; Kane et al. 2021). Despite their similar radii ($\sim$ 1.0–1.1 $R_\oplus$), the two planets experience distinct space weather environments due to their different orbital distances from the M5V host star, likely leading to divergent atmospheric evolution pathways (Dong et al. 2018). While previous studies have characterized atmospheric loss in M-dwarf systems based on either stellar winds and radiation at the current epoch or limited evolutionary stages (Dong et al. 2017, 2018, 2020; Cohen et al. 2020; Modi et al. 2023), the effects of long-term stellar evolution on non-thermal atmospheric erosion over gigayear timescales remain unexplored. This gap is particularly significant for systems like Kepler 1649, where two Earth-sized planets at distinct orbits offer a unique opportunity to study divergent atmospheric evolution pathways under sustained stellar influences.

This study aims to quantify the time-dependent ion escape from Kepler-1649 b and c to to assess their potential for atmospheric retention throughout the host star's evolution. This investigation contributes to our understanding of exoplanet habitability by characterizing atmospheric loss around M-dwarfs, a class of stars that host many known terrestrial planets. Its significance lies in bridging theoretical models with future observations, such as those enabled by the James Webb Space Telescope (JWST) (Santos et al. 2023), which may detect atmospheric signatures like CO_2 (Madhusudhan et al. 2023). By assessing whether these planets can sustain atmospheres over gigayear timescales, this work addresses a key criterion for habitability and enhances the interpretation of upcoming spectroscopic observations (Lustig-Yaeger et al. 2022; Yang & Hu 2024).

In this work, we employ a multi-species MHD model to simulate ion escape from Kepler-1649 b and c over 0.7 to 4.8 Gyrs. Our approach incorporates: (1) time-dependent stellar wind parameters derived from rotational braking models (Ribas et al. 2017), and (2) EUV flux evolution calibrated to M-dwarf activity cycles (Varela et al. 2023). This enables quantitative predictions of atmospheric erosion under realistic stellar evolutionary scenarios. The structure of this Letter is arranged as follows. In Section 2, we provide a detailed description of the simulation setup, including the calculation of various parameters essential for the simulations. Subsequently, we present the results obtained from the simulations in Section 3. Finally, we summarize our findings based on the analysis in Section 4.

2. THE SIMULATION SETUP

In this section, we present the numerical model used for our simulations, as well as the methods used to calculate the required input parameters.

2.1. *Simulation Parameters*

To simulate stellar winds is challenging. The latest models (e.g., Cohen et al. 2023) incorporate three-dimensional self-consistent approaches. However, these

models often require knowledge of the stellar magnetic field maps as input to simulate stellar winds. In the absence of observed magnetic maps for Kepler-1649, we adopt the Parker stellar wind model to calculate the stellar wind parameters. Such assumptions have also been made in previous research (See et al. 2014; Modi et al. 2023). The calculation is performed in the spherical coordinate system, and we convert the results to Cartesian coordinates and use them for subsequent simulation (Section A in the Appendix). The calculated data are listed in Table 1. We calculate the stellar wind parameters and interplanetary magnetic field (IMF) of Kepler-1649 using the stellar radius ($0.22 \, R_\odot$) and mass ($0.25 \, M_\odot$) reported by Angelo et al. (2017). The rotational period at different ages was calculated using empirical relations from Modi et al. (2023). Due to the lack of direct observations of the surface magnetic field for Kepler-1649, we derive an age-dependent estimate of the surface magnetic field through interpolation based on simulation results from Landin et al. (2023), which is essential for estimating the IMF.

We estimate the age of Kepler-1649 from MESA isochrones v1.2 (Paxton et al. 2011; Dotter 2016). The stellar parameters of Kepler-1649 were taken from Vanderburg et al. (2020). The age of Kepler-1649 was estimated by matching its stellar parameters (with uncertainties) to a set of isochrones with a stellar mass of $0.2 \, M_\odot$ but varying metallicities covering the range of [Fe/H]=-0.15±0.11. The best fit isochrone results in $\log_{10} \tau \sim 9.3$, which corresponds to the age τ of Kepler-1649 ~ 2.0 Gyrs.

Because the spectral type of Kepler-1649 is M5V (Angelo et al. 2017), we use the spectral data of GJ 551 with a spectral type of M5.5V from MUSCLES (France et al. 2016) as the spectrum of Kepler-1649. We scale the spectrum at the surface of the Kepler-1649 to obtain fluxes at the positions of Kepler-1649 b and c, which are input parameters for photoionization (see Figure 4 in the Appendix). For the different ages of Kepler-1649, we employ the relationship given by Ribas et al. (2017) for the temporal evolution of GJ 551 X-ray and extreme-ultraviolet (XUV) flux ($F_{\rm XUV}$ in $\rm Wm^{-2}$, τ in Myr)

$$F_{\rm XUV} = \begin{cases} 84.1\tau^{-0.71} & 10 < \tau < 300, \\ 1.47 & 300 < \tau < 1640, \\ 9.74 \times 10^4 \tau^{-1.5} & 1640 < \tau < 4800. \end{cases} \quad (1)$$

Using this relationship, we obtain the evolved stellar spectrum and calculate the photoionization rates (Section C in the Appendix). Incorporating GJ 551's time dependent spectral data and the ionization cross sections of CO_2 and O, we derive the photoionization rates for different stellar ages. Combining the inverse square relationship between XUV flux and the orbital radius, we derive the photoionization rates of Kepler-1649 b and c, which are listed in Table 1.

To define the temporal scope of our time-dependent ion escape simulations, we establish a starting point of 0.7 Gyr and an upper bound of 4.8 Gyrs, reflecting both astrophysical constraints and habitability considerations. The choice of 4.8 Gyrs as the endpoint is motivated by the significant uncertainty in Kepler-1649's age, yet potentially ranging up to several gigayears due to ambiguities in M-dwarf evolutionary tracks and metallicity variations (Paxton et al. 2011; Modi et al. 2023). We adopt a timeline comparable to that of the Solar System, where the emergence of complex life and the stabilization of a modern atmosphere demanded nearly the entirety of Earth's evolutionary history. This cutoff emphasizes the critical role of prolonged atmospheric retention in habitability assessments for terrestrial exoplanets, as the development of conditions supportive of complex life likely requires billions of years of atmospheric stability (Schwieterman et al. 2018). The starting time of 0.7 Gyr is set due to the limitations of the stellar wind evolution model (Section A in the Appendix), which becomes increasingly unreliable for ages $\lesssim 0.7$ Gyr (Wood et al. 2005; Popinchalk et al. 2021; Modi et al. 2023). By initiating at 0.7 Gyr, we ensure the simulation captures a physically realistic baseline for atmospheric erosion while avoiding extrapolation into poorly constrained early stellar phases.

Due to the harsh space environment to which Kepler-1649 b and c are exposed, they might undergo processes similar to Venus during the early stages of atmospheric evolution, leading to significant loss of water and H_2, resulting in CO_2 and O becoming the predominant neutral constituents of their atmospheres (Angelo et al. 2017). Furthermore, we calculate the neutral atmosphere by scaling the neutral atmosphere of Venus following Dong et al. (2017). The Venusian neutral atmosphere[1] from Ma et al. (2013) is

$$[CO_2] = 1.0 \cdot 10^{15} \cdot e^{-(z-z_0)/5.5} \, \rm cm^{-3}, \quad (2)$$

$$[O] = 2.0 \cdot 10^{11} \cdot e^{-(z-z_0)/17} \, \rm cm^{-3}, \quad (3)$$

where $z_0 = 100$ km. Studies have shown that ion escape rates exhibit a weak dependence on surface pressure (Dong et al. 2017). Since the surface pressure is currently unknown, we assume that the surface atmospheric pressure of Kepler-1649 b and c is 1 bar (Dong et al. 2017). Thus, we obtain a density that is 0.011 times the Venus value at the model lower boundary. Next, we assume that only the gravity changes, the scale heights of Kepler-1649 b and c are

$$H_{\rm Kepler-1649b} = \frac{kT}{mg} = 0.89 H_{\rm Venus}, \quad (4)$$

$$H_{\rm Kepler-1649c} = \frac{kT}{mg} = 0.84 H_{\rm Venus}. \quad (5)$$

---

[1] The scale height of Venus $H_{\rm Venus}$ is 5.5 km for CO_2 and 17 km for O.

The planetary parameters of Kepler-1649 b and c are taken from Vanderburg et al. (2020).

2.2. *MHD model and setup*

In the previous subsection, we introduce the method used to calculate the stellar wind parameters, the IMF, the XUV flux and resulting photoionization rate. In this subsection, we will describe the MHD model used for the subsequent simulations and the parameters we have adopted.

We use the 3D Block Adaptive Tree Solar-Wind Roe Up-Wind Scheme (BATS-R-US) multi-species MHD (MS-MHD) model (Tóth et al. 2012) to simulate the stellar wind interaction with Kepler-1649 b and c. BATS-R-US has many modules for simulating different physical phenonmena. This model has been successfully applied to simulate atmospheric ion escale for Venus-like exoplanets (Dong et al. 2017, 2018, 2020). The MS-MHD model solves four continuity equations for each ion species which are H^+, O^+, O_2^+, and CO_2^+, and treats each ion species as a fluid, requiring one momentum equation and one energy equation (Ma et al. 2013). This model self-consistently includes photoionization, charge exchange, and electron recombination. Due to the lack of direct observations, we assume that the atmospheric compositions of Kepler-1649 b and c are close to that of Venus (Angelo et al. 2017). The reaction rates used for the simulations are listed in Table 3 (Section C in the Appendix).

We adopt a nonuniform grid to ensure that the radial resolution inside the ionosphere is 5 km, while the outer boundary resolution is thousands of kilometers. The angular resolution is 3°. For the coordinate system, the positive direction of the x axis is directed from the planet to the star. The z axis is perpendicular to the orbital plane, and the y axis constitutes a right-hand system. The computational domain is defined by $-20\,R_P \leq X \leq 12\,R_P$, $-16\,R_P \leq Y, Z \leq 16\,R_P$, where R_P is the radius of the planet.

3. RESULTS

This section presents the calculated ion escape rates for the Kepler-1649 system. We first establish the stellar age dependence of ion escape rates through power-law parameterizations, then examine spatial ion distribution changes in response to evolving stellar wind and radiation conditions. Comparative analysis between Kepler-1649 b and c reveals how orbital distance modulate erosion efficiency across gigayear timescales.

Figure 1 and Table 2 present the temporal evolution of atmospheric ion escape rates for Kepler-1649 b and c across 0.7–4.8 Gyrs, simulated under varying stellar wind and XUV radiation conditions. The data reveal escape rates spanning four orders of magnitude (10^{23}–10^{27} s^{-1}), quantified through multi-species MHD

simulations using a 10 R_P integration sphere. Both planets exhibit systematic declines in O^+, O_2^+, and CO_2^+ escape fluxes with stellar age, with total rates decreasing from 1.9×10^{27} s^{-1} (Kepler-1649 b) and 1.0×10^{27} s^{-1} (Kepler-1649 c) at 0.7 Gyr to 3.0×10^{25} s^{-1} for both planets at 4.8 Gyrs. Table 2 presents the calculated different ion escape rates at 12 evolutionary stages, allowing a direct comparison of absolute values and relative ion contributions.

Figure 1 displays the temporal evolution of ion escape rates for Kepler-1649 b (left panels) and c (right panels) across stellar ages (0.7–4.8 Gyrs). The escape rates of both planets follow a power-law decay over time for all ion species (O^+, O_2^+, CO_2^+, and total) with distinct exponents. For Kepler-1649 b, the fitted power-law indices (α) are $\alpha_{O^+} = -1.51$, $\alpha_{O_2^+} = -3.02$, and $\alpha_{CO_2^+} = -2.98$, indicating that O_2^+ escape shows the strongest age dependence. In contrast, our results for Kepler-1649 c are $\alpha_{O^+} = -1.36$, $\alpha_{O_2^+} = -2.03$, and $\alpha_{CO_2^+} = -2.71$, with CO_2^+ showing the steepest decline. Total escape rates follow intermediate trends ($\alpha_{\text{total,Kepler}-1649\text{ b}} = -1.62$, $\alpha_{\text{total,Kepler}-1649\text{ c}} = -1.46$), reflecting combined contributions from all species. At 0.7 Gyr, Kepler-1649 b's total escape rate (1.9×10^{27} s^{-1}) exceeds Kepler-1649 c's (1.0×10^{27} s^{-1}) by a factor of 1.9, a disparity maintained throughout their evolution. Regarding the early-time behavior in Figure 1 (e.g., O^+ escape rate at 0.7 Gyr), we confirm that the initial scatter in the ion escape rates (t $\lesssim$ 0.7 Gyr) is indeed influenced by uncertainties in reconstructing the stellar wind evolution for young stars. As noted, the current stellar wind evolution models exhibit limited precision for ages $\lesssim$0.7 Gyr due to the observed dispersion in rotation period rates of young M dwarfs $\lesssim$0.7 Gyr (Popinchalk et al. 2021). This scatter propagates into uncertainties in early stellar wind mass-loss rates, which directly affect atmospheric ion escape (Wood et al. 2005; Modi et al. 2023).

Table 2 quantifies the dominance of O^+ in atmospheric loss. For Kepler-1649 b, O^+ contributes 76.8%–98.7% of the total escape flux across all ages, while O_2^+ and CO_2^+ contribute 0.8%–17.9% and 0.6%–5.4%, respectively. Similarly, O^+ accounts for 77.1%–93.0% of Kepler-1649 c's total escape, with O_2^+ and CO_2^+ contributing 5.8%–18.9% and 1.2%–6.6%. The O^+ escape rate for both planets decreases by about two orders of magnitude over 4.1 Gyrs (1.4×10^{27} s^{-1} to 3.0×10^{25} s^{-1} for Kepler-1649 b; 7.8×10^{26} s^{-1} to 2.8×10^{25} s^{-1} for Kepler-1649 c). Notably, Kepler-1649 b maintains higher O^+ escape rates than Kepler-1649 c at all epochs, with the ratio $R_{O^+,\text{Kepler}-1649\text{ b}}/R_{O^+,\text{Kepler}-1649\text{ c}}$ ranging from 1.9 at 0.7 Gyr to 1.1 at 4.8 Gyrs.

Figures 2 and 3 illustrate the temporal evolution of ion escape patterns for Kepler-1649 b and c across 0.7–4.8 Gyrs, highlighting two key trends: (1) significantly higher ion escape rates in the early evolutionary stages due to intense stellar winds and XUV radiation, and
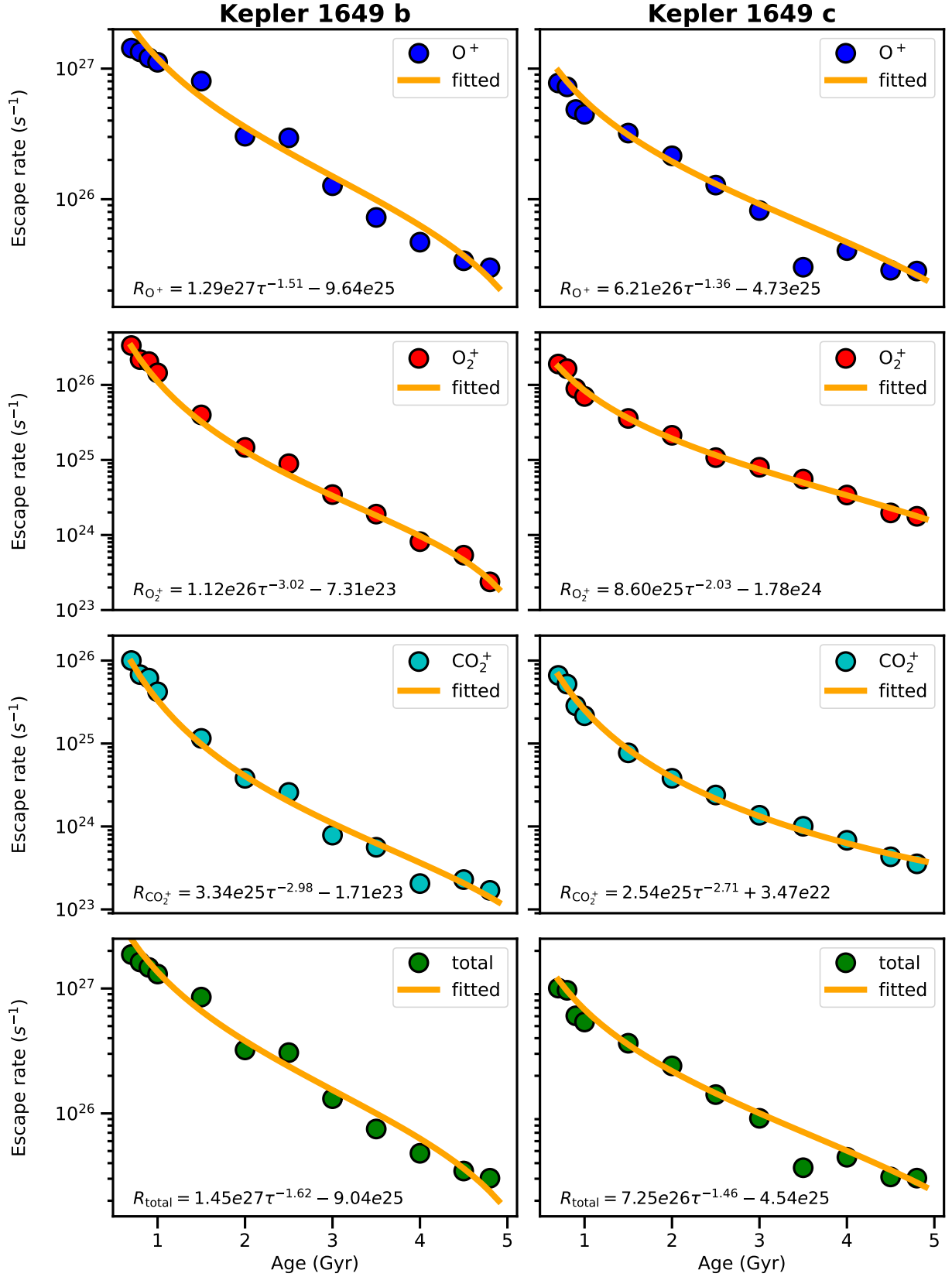
Figure 1. Evolution of ion escape rates for Kepler-1649 b (left panels) and c (right panels) across stellar ages (0.7–4.8 Gyrs). Top to bottom: O^+, O_2^+, CO_2^+, and total ion escape rates (s^{-1}). Data points are fitted with power-law functions (solid lines).

Table 1. Stellar wind parameters and photoionization rates for Kepler-1649 b and c.

Age (Gyr)	N_{sw} (cm^{-3})	T_{sw} (K)	V_{sw} (km/s)	IMF (nT)	q_{CO_2} (s^{-1})	q_O (s^{-1})
			Kepler-1649 b			
0.7	3105	2.01×10^6	(-632, 0, 0)	(-426.276, -0.429, 0)	1.10×10^{-4}	4.15×10^{-5}
0.8	2580	1.84×10^6	(-597, 0, 0)	(-399.908, -0.381, 0)	1.10×10^{-4}	4.15×10^{-5}
0.9	2190	1.71×10^6	(-568, 0, 0)	(-382.330, -0.347, 0)	1.10×10^{-4}	4.15×10^{-5}
1.0	1891	1.59×10^6	(-542, 0, 0)	(-364.752, -0.316, 0)	1.10×10^{-4}	4.15×10^{-5}
1.5	1074	1.22×10^6	(-455, 0, 0)	(-307.622, -0.223, 0)	1.10×10^{-4}	4.15×10^{-5}
2.0	720	1.01×10^6	(-402, 0, 0)	(-272.465, -0.174, 0)	8.18×10^{-5}	3.07×10^{-5}
2.5	528	8.69×10^5	(-365, 0, 0)	(-246.097, -0.142, 0)	5.85×10^{-5}	2.20×10^{-5}
3.0	410	7.71×10^5	(-338, 0, 0)	(-228.519, -0.121, 0)	4.45×10^{-5}	1.67×10^{-5}
3.5	331	6.97×10^5	(-316, 0, 0)	(-219.730, -0.108, 0)	3.53×10^{-5}	1.33×10^{-5}
4.0	276	6.39×10^5	(-299, 0, 0)	(-206.546, -0.096, 0)	2.89×10^{-5}	1.09×10^{-5}
4.5	234	5.91×10^5	(-285, 0, 0)	(-197.757, -0.087, 0)	2.42×10^{-5}	9.11×10^{-6}
4.8	215	5.67×10^5	(-278, 0, 0)	(-188.968, -0.081, 0)	2.20×10^{-5}	8.27×10^{-6}
			Kepler-1649 c			
0.7	964	2.01×10^6	(-684, 0, 0)	(-144.732, -0.230, 0)	3.75×10^{-5}	1.41×10^{-5}
0.8	799	1.84×10^6	(-647, 0, 0)	(-135.780, -0.204, 0)	3.75×10^{-5}	1.41×10^{-5}
0.9	677	1.71×10^6	(-615, 0, 0)	(-129.811, -0.185, 0)	3.75×10^{-5}	1.41×10^{-5}
1.0	583	1.59×10^6	(-588, 0, 0)	(-123.843, -0.169, 0)	3.75×10^{-5}	1.41×10^{-5}
1.5	328	1.22×10^6	(-495, 0, 0)	(-104.446, -0.118, 0)	3.75×10^{-5}	1.41×10^{-5}
2.0	218	1.01×10^6	(-437, 0, 0)	(-92.509, -0.091, 0)	2.78×10^{-5}	1.04×10^{-5}
2.5	159	8.69×10^5	(-397, 0, 0)	(-83.557, -0.074, 0)	1.99×10^{-5}	7.47×10^{-6}
3.0	123	7.71×10^5	(-367, 0, 0)	(-77.588, -0.063, 0)	1.51×10^{-5}	5.68×10^{-6}
3.5	99	6.97×10^5	(-343, 0, 0)	(-74.604, -0.056, 0)	1.20×10^{-5}	4.51×10^{-6}
4.0	82	6.39×10^5	(-324, 0, 0)	(-70.128, -0.049, 0)	9.82×10^{-6}	3.69×10^{-6}
4.5	69	5.91×10^5	(-308, 0, 0)	(-67.144, -0.044, 0)	8.23×10^{-6}	3.09×10^{-6}
4.8	63	5.67×10^5	(-300, 0, 0)	(-64.160, -0.041, 0)	7.47×10^{-6}	2.81×10^{-6}
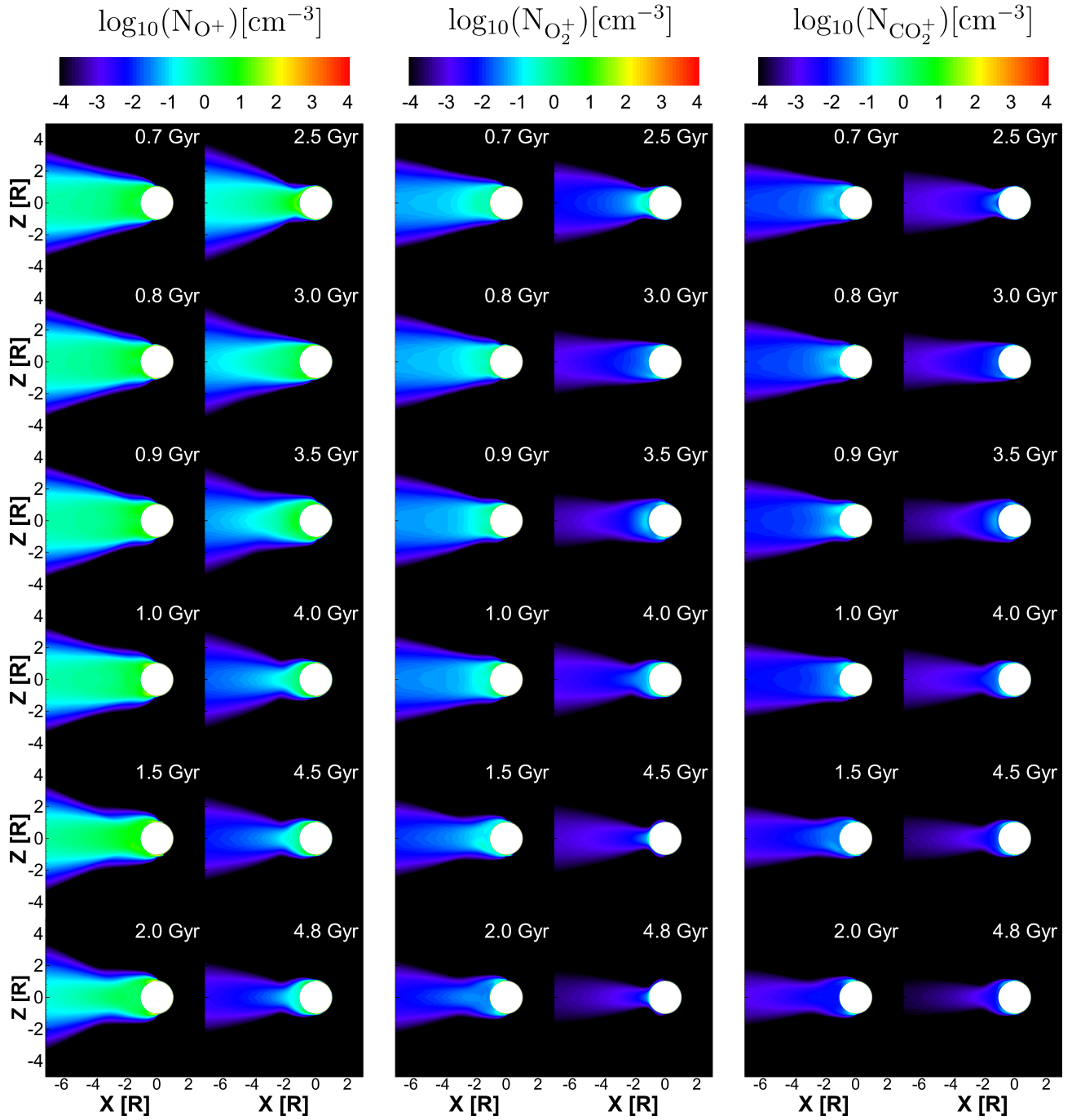
Figure 2. Logarithmic ion number density (cm^{-3}) distributions in the X-Z plane for Kepler-1649 b at different stellar ages (0.7–4.8 Gyrs; top to bottom). Columns show O$^+$, O$_2$$^+$, and CO$_2$$^+$ (left to right). Coordinates are normalized to planetary radius R_P.

Table 2. The calculated atmospheric ion escape rates (of different ion species) in units of $\sec^{-1}$ as a function of stellar age for Kepler-1649 b and c.

Age (Gyr)	O^+	O_2^+	CO_2^+	Total
		Kepler-1649 b		
0.7	1.434×10^{27}	3.345×10^{26}	1.001×10^{26}	1.869×10^{27}
0.8	1.343×10^{27}	2.172×10^{26}	6.769×10^{25}	1.628×10^{27}
0.9	1.208×10^{27}	2.046×10^{26}	6.143×10^{25}	1.474×10^{27}
1.0	1.118×10^{27}	1.446×10^{26}	4.203×10^{25}	1.305×10^{27}
1.5	8.018×10^{26}	3.982×10^{25}	1.153×10^{25}	8.531×10^{26}
2.0	3.038×10^{26}	1.469×10^{25}	3.806×10^{24}	3.222×10^{26}
2.5	2.952×10^{26}	8.919×10^{24}	2.573×10^{24}	3.067×10^{26}
3.0	1.270×10^{26}	3.457×10^{24}	7.856×10^{23}	1.312×10^{26}
3.5	7.258×10^{25}	1.898×10^{24}	5.614×10^{23}	7.504×10^{25}
4.0	4.692×10^{25}	8.154×10^{23}	2.049×10^{23}	4.794×10^{25}
4.5	3.382×10^{25}	5.384×10^{23}	2.289×10^{23}	3.459×10^{25}
4.8	2.988×10^{25}	2.375×10^{23}	1.698×10^{23}	3.029×10^{25}
		Kepler-1649 c		
0.7	7.761×10^{26}	1.899×10^{26}	6.626×10^{25}	1.006×10^{27}
0.8	7.251×10^{26}	1.641×10^{26}	5.206×10^{25}	9.670×10^{26}
0.9	4.862×10^{26}	8.950×10^{25}	2.855×10^{25}	6.043×10^{26}
1.0	4.472×10^{26}	7.009×10^{25}	2.162×10^{25}	5.389×10^{26}
1.5	3.209×10^{26}	3.574×10^{25}	7.712×10^{24}	3.644×10^{26}
2.0	2.151×10^{26}	2.131×10^{25}	3.808×10^{24}	2.402×10^{26}
2.5	1.283×10^{26}	1.074×10^{25}	2.396×10^{24}	1.415×10^{26}
3.0	8.201×10^{25}	7.986×10^{24}	1.365×10^{24}	9.137×10^{25}
3.5	3.019×10^{25}	5.558×10^{24}	1.004×10^{24}	3.675×10^{25}
4.0	4.050×10^{25}	3.410×10^{24}	6.809×10^{23}	4.459×10^{25}
4.5	2.862×10^{25}	1.968×10^{24}	4.308×10^{23}	3.102×10^{25}
4.8	2.821×10^{25}	1.774×10^{24}	3.544×10^{23}	3.034×10^{25}
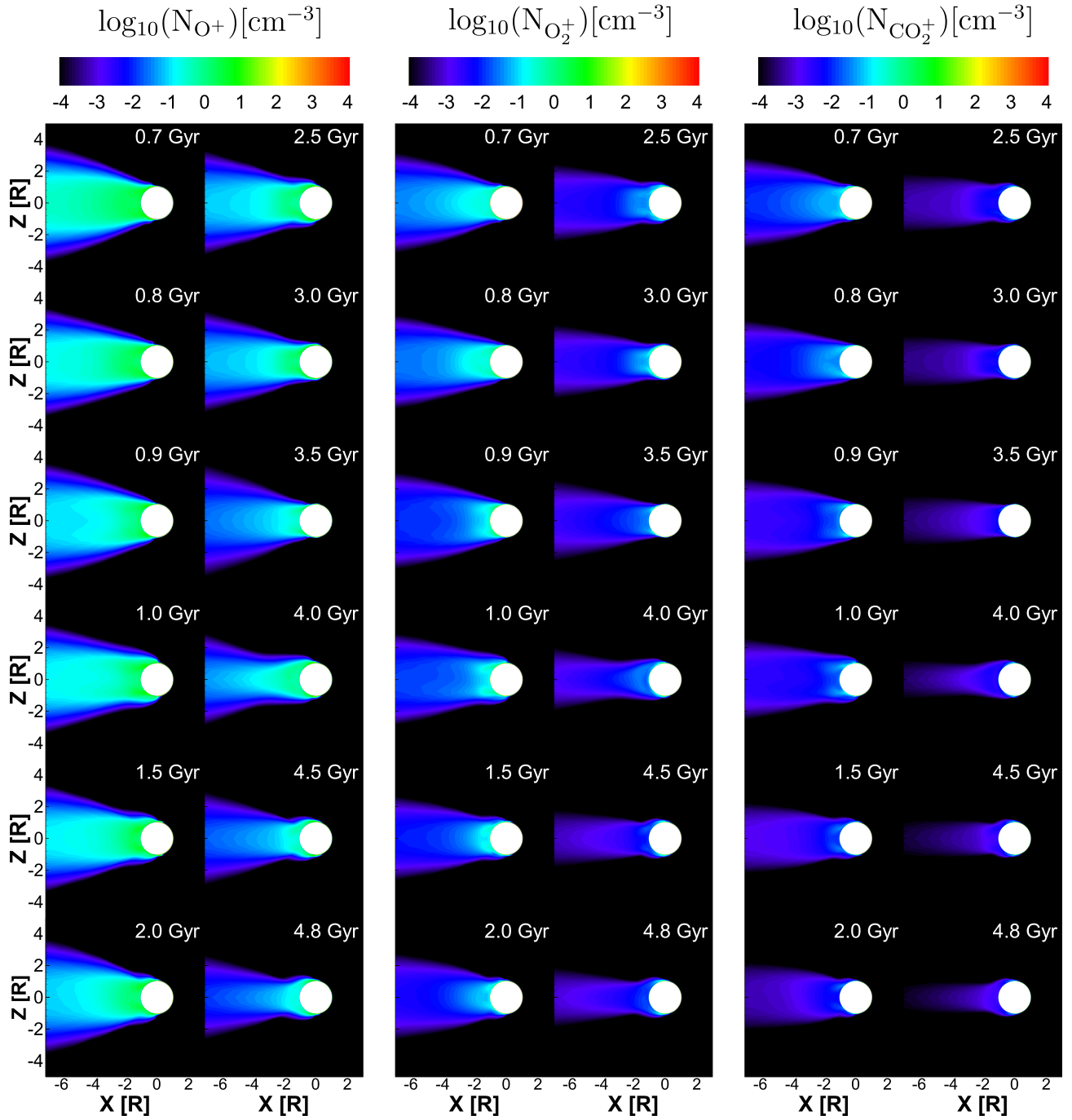
Figure 3. Logarithmic ion number density (cm^{-3}) distributions in the X-Z plane for Kepler-1649 c at different stellar ages (0.7–4.8 Gyrs; top to bottom). Columns show O$^+$, O$_2^+$, and CO$_2^+$ (left to right). Coordinates are normalized to planetary radius R_P.

(2) the dominance of O^+ in the escaping ion flux across all epochs. Both planets exhibit systematically higher ion densities and more extended ionospheres at younger stellar ages, particularly for O^+, which dominates the escaping flux. The dominance of O^+ escape is visually evident in the extended ion tails in Figures 2 and 3. This early high escape is supported by the dense ionospheric structures (see Figures 5 and 6 in the Appendix), where elevated dayside O^+ densities enhance ion loss, driven by the strong XUV flux and stellar wind pressure in the early epochs. Comparative analysis shows that Kepler-1649 b exhibits higher dayside ionospheric densities than Kepler-1649 c, driven by stronger stellar radiation due to its closer orbital distance. These findings highlight the critical influence of orbital proximity (0.051 AU for Kepler-1649 b vs. 0.088 AU for Kepler-1649 c) and stellar evolution in regulating atmospheric loss. Overall, the results demonstrate that the atmospheric erosion histories of M-dwarf planets are shaped by both orbital distance and the evolving stellar wind and radiation environment.

4. DISCUSSION AND CONCLUSION

This work investigates the long-term atmospheric retention of Kepler-1649 b and c throughout the evolutionary history of their M-dwarf host, tackling a key challenge in assessing exoplanet habitability. We employed a well-validated multi-species magnetohydrodynamic (MHD) model to simulate time-dependent ion escape driven by stellar winds and extreme ultraviolet (EUV) radiation across 0.7–4.8 Gyrs. Our focus on these Earth-sized planets offers a unique opportunity to probe atmospheric retention under M-dwarf conditions, where stellar activity strongly influences planetary evolution. Expanding on previous research, this study provides an evolutionary context for atmospheric loss, yielding fundamental insights into the persistence of terrestrial exoplanet atmospheres orbiting active M-dwarfs.

The power-law decay model captures the dynamical evolution of atmospheric escape in active M-dwarf systems. The observed $\tau^{-1.6}$ ($\tau^{-1.5}$) power-law decay of total ion escape rates (Fig. 1) arises from the decline of both stellar wind dynamic pressure ($P_{\rm dyn} \propto \tau^{-2.1}$) and XUV flux ($F_{\rm XUV} \propto \tau^{-0.7} \sim \tau^{-1.5}$), as predicted by M-dwarf rotational braking models (Ribas et al. 2017). Correspondingly, escape rates decrease from 1.9×10^{27} s^{-1} and 1.0×10^{27} s^{-1} at 0.7 Gyr to 3.0×10^{25} s^{-1} for Kepler-1649 b and c, respectively, at 4.8 Gyrs. The power-law decline in ion escape rates from 0.7 to 4.8 Gyrs highlights the critical influence of stellar evolution on the atmospheric retention of Kepler-1649 b and c. This trend aligns with the expected weakening of stellar activity in M-dwarfs, where early epochs are marked by intense high-energy radiation and particle fluxes that drive significant atmospheric erosion, while later stages allow for increased atmospheric stability (Zendejas et al. 2010; France et al. 2020).

The differences in atmospheric ion escape rates between Kepler-1649 b and c arise from their orbital separations and the evolving stellar wind and XUV radiation environment. At 0.7 Gyr, Kepler-1649 b (0.051 AU) exhibits a total ion escape rate of 1.9×10^{27} s^{-1}, 1.9 times higher than Kepler-1649 c's 1.0×10^{27} s^{-1} (0.088 AU), a disparity rooted in the inverse-square scaling of stellar wind dynamic pressure and XUV flux (Ribas et al. 2017). Based on the calculation, the cumulative O^+ loss for Kepler-1649 b reaches 4.74×10^{43} ions (equivalent to 0.24 bar) over the 0.7–4.8 Gyrs period. This suggests that both Kepler-1649 b and Kepler-1649 c—with the latter experiencing approximately half the integrated loss—could retain a 1 bar CO_2-dominated atmosphere for several billion years. These findings imply that M-dwarf planets may be capable of sustaining atmospheres conducive to long-term habitability. This study builds on prior work by quantifying time-dependent escape throughout the evolutionary history of a star. Our power-law fits ($\alpha_{\rm total} = -1.62$ for Kepler-1649 b, -1.46 for Kepler-1649 c) provide insights into atmospheric loss in habitable-zone planets around M-dwarfs.

We note that our model assumes fixed circular orbits without planet-planet interactions. However, even if both orbits are initially circular, they are going to become eccentric (e.g., Georgakarakos 2003, 2009), thus altering star-planet distances and possibly atmospheric erosion rates. Although the planetary eccentricities of the specific system are not known, some constraints, however, can arise from the fact that the system must be dynamically stable. Assuming initially circular orbits for both Kepler-1649 b and c, the stability results of hierarchical triple systems given in Georgakarakos (2013) indicate that a system such as Kepler-1649 would be fairly stable. Nonetheless, if any of the planets is on a mildly eccentric orbit, both secular and resonant oscillations (our system is close to a 9:4 mean motion resonance) may become more significant for the dynamical evolution the system. Assuming a circular orbit for Kepler-1649b, Kane et al. (2021) found that the system became unstable when the eccentricity of Kepler-1649c had an initial eccentricity beyond 0.325 in their numerical experiments. Future work should address how orbital distance variability impacts long-term atmospheric retention in this system.

Future investigations should also incorporate dynamic atmospheric models and additional physical processes to enhance the model's predictive power. Adopting time-evolving photochemical models (Tsai et al. 2017; Cangi & Chaffin 2024) would capture neutral atmosphere evolution, addressing the static assumption's shortcomings. Including planetary magnetic field evolution, as in Carolan et al. (2021), could reveal shielding effects on ion escape. Three-dimensional stellar wind models (Garraffo et al. 2022; Cohen et al. 2023) would better resolve spatial variability, while integrating secondary ionization (Gillet et al. 2023), kinetic processes (Strangeway

et al. 2005) and outgassing (Schaefer & Fegley 2007; Kite et al. 2016; Wordsworth & Kreidberg 2022; Teixeira et al. 2024) would provide a holistic view of atmospheric budgets. Constraining Kepler-1649's age with multi-method stellar chronology (e.g., gyrochronology, isochrones) would further anchor the evolutionary timeline, refining habitability predictions for these exoplanets.

In summary, this Letter highlights several key findings. The atmospheric ion escape rates for Kepler-1649 b and c exhibit a power-law decline with stellar age. Both planets appear capable of retaining their atmospheres over 4.8 Gyrs, carrying important implications for their potential habitability. The results emphasize the crucial role of orbital distance and stellar evolution in regulating atmospheric retention and evolution, offering a benchmark for interpreting upcoming JWST observations of M-dwarf exoplanets.

APPENDIX

A. PARKER'S STELLAR WIND MODEL

The Parker's wind equation is read as (Priest 2012; Grießmeier 2007)

$$\left(\frac{v(d)}{v_{\text{crit}}}\right)^2 - 2\ln\left(\frac{v(d)}{v_{\text{crit}}}\right)^2 = 4\ln\frac{d}{r_{\text{crit}}} + 4\frac{r_{\text{crit}}}{d} - 3. \tag{A1}$$

By solving this equation, the stellar wind velocity $v(d)$ at distance d can be obtained. The critical velocity v_{crit} is defined as

$$v_{\text{crit}} = \sqrt{\frac{k_{\text{B}}T}{m}}, \tag{A2}$$

and the critical radius r_{crit} is

$$r_{\text{crit}} = \frac{mGM_*}{4k_{\text{B}}T}. \tag{A3}$$

We can also calculate the density $n(r)$ of the stellar wind by

$$n(r) = \frac{\dot{M}_*}{4\pi d^2 v(d)m}. \tag{A4}$$

Here, k_{B} is the Boltzmann constant, T is the temperature of the stellar wind, m is the mass of the stellar wind protons, G is the gravitational constant, and $\dot{M}_* = 4\pi d^2 v(d)m$ is the stellar mass loss rate. To validate these formulas, we perform calculations for the Sun's stellar wind velocity and number density at 1 AU. The results yield approximately 422 km/s and 6.62 cm^{-3}, respectively, which are consistent with observations obtained from spacecrafts such as SOHO and vela-3. It is noteworthy that the method in Grießmeier (2007) limits a stellar age greater than 0.7 Gyr. For younger stars, the stellar wind dynamic pressure is actually much stronger than that obtained by this method, which is why we chose 0.7 Gyr as the lower limit on the time point.

Grießmeier (2007) provided a method for calculating solar wind parameters of M-type stars based on the formula mentioned above. Using a set of M-type stars with a standard orbital radius of 1 AU and a stellar age of 4.6 Gyrs, we iteratively adjust the coronal temperature until the velocity derived from Eq. (A1) matches the standard value. Subsequently, we substitute the obtained coronal temperature into Eqs. (A2) and (A3) to calculate the stellar wind

speed for the target radius and stellar age. Finally, we use the obtained velocity in Eq. (A4) to compute the density. The calculated results are listed in Table 1. Within 1 AU, as the distance increases, the stellar wind density decreases while the velocity increases, which is consistent with the results from Grießmeier (2007).

The IMF is calculated with the equations (Parker 1958)

$$B_r(r, \theta, \phi) = B(\theta, \phi_0) \left(\frac{b}{r}\right)^2 , \tag{A5}$$

$$B_\theta(r, \theta, \phi) = 0, \tag{A6}$$

$$B_\phi(r, \theta, \phi) = B(\theta, \phi_0) \left(\frac{\omega}{v_m}\right) (r - b) \left(\frac{b}{r}\right)^2 \sin(\theta). \tag{A7}$$

These equations use a spherical coordinate system centered on the star to describe the decay of the IMF with the $1/r^2$, where r is the distance between the target position and the star, b is a distance beyond which the solar gravitation, $B(\theta, \phi_0)$ is the magnetic field at $r = b$, ω is the angular velocity of Kepler-1649, which can calculate by empirical relations from Modi et al. (2023). If only the dipole magnetic field of the star is considered, $B(\theta, \phi_0)$ can be considered as the vertical component of the surface magnetic field at the planet. By substituting the calculated stellar wind velocities obtained from the previous section into the equations, the stellar wind magnetic field parameters for different stellar ages are obtained.

B. STELLAR SPECTRA
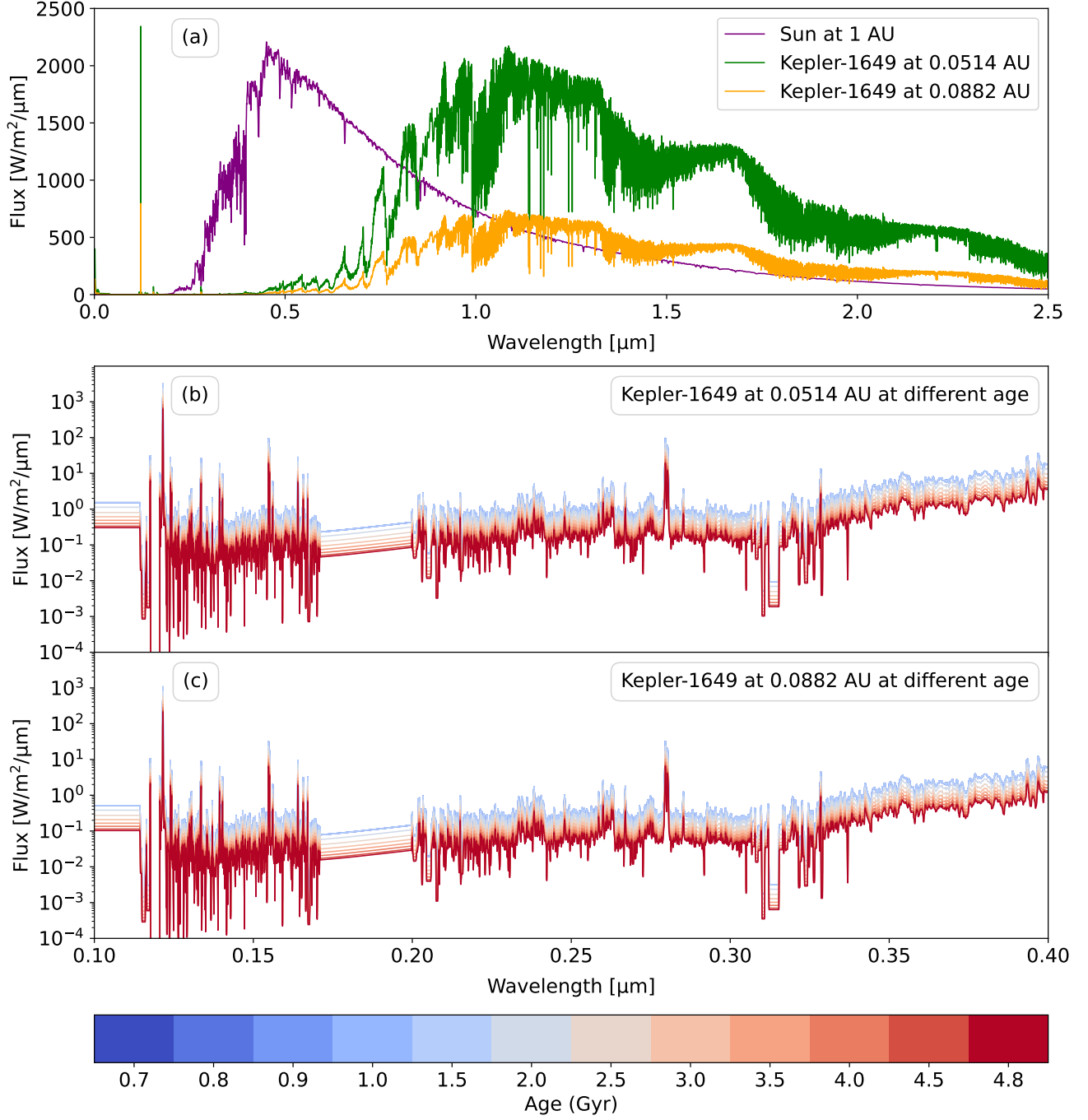
Figure 4. Stellar spectra comparison at 4.8 Gyrs. Panel (a): flux (W m^{-2} μm) for Kepler-1649 at the orbital distances of planets b (0.0514 AU, green line) and c (0.0882 AU, orange line), compared to the solar spectrum at Earth (purple line). Kepler-1649's spectrum is scaled from Proxima Centauri (M5.5V), matching its spectral type. Panels (b) and (c): the temporal evolution of the EUV flux (100 nm–400 nm, W m^{-2} μm) for Kepler-1649 at the orbital distances of planets b and c, respectively, spanning stellar ages of 0.7 to 4.8 Gyrs.

C. CHEMICAL REACTIONS AND RELATED RATES

We calculated the photoionization rates using the equation (Torr & Torr 1985)

$$q_i = \int_\lambda \sigma_i(\lambda) F_\infty(\lambda) d\lambda, \tag{C8}$$

where σ_i is the ionization cross-section and F_∞ is the radiative flux at the top of the atmosphere. By integrating the product of these quantities over wavelength, we determined the photoionization rates as input parameters.

Table 3. Chemical Reactions and related rates.

Chemical Reaction	Rate Coefficient[a]
Primary Photolysis[b] in s^{-1}	
$CO_2 + h\nu \rightarrow CO_2{}^+ + e^-$	see Table 1
$O + h\nu \rightarrow O^+ + e^-$	see Table 1
Ion-neutral and electron recombination chemistry in $cm^3\,s^{-1}$	
$CO_2{}^+ + O \rightarrow O_2{}^+ + CO$	1.64×10^{-10}
$CO_2{}^+ + O \rightarrow O^+ + CO_2$	9.60×10^{-11}
$O^+ + CO_2 \rightarrow O_2{}^+ + CO$	$1.1 \times 10^{-9}\ (800/T_i)^{0.39}$
$H^+ + O \rightarrow O^+ + H^c$	5.08×10^{-10}
$O_2{}^+ + e^- \rightarrow O + O$	$7.38 \times 10^{-8}\ (1200/T_e)^{0.56}$
$CO_2{}^+ + e^- \rightarrow CO + O$	$3.10 \times 10^{-7}\ (300/T_e)^{0.5}$

[a] The reaction rates are based on Schunk & Nagy (2009), with electron impact ionization omitted in the calculations. The H^+ density is sourced from the stellar wind, and neutral hydrogen is disregarded.

[b] The photoionization rates are derived and scaled to correspond to Kepler-1649 b and c, employing the EUV flux calculated through Eq. (1).

[c] The rate coefficient is adopted from Fox & Sung (2001).

D. O^+ AND $O_2{}^+$ DISTRIBUTION IN THE DAYSIDE IONOSPHERE AT 0.7 GYR AND 4.8 GYRS

The logarithmic distributions of O^+ and $O_2{}^+$ in the dayside ionosphere of Kepler-1649 b and Kepler-1649 c at 0.7 Gyr and 4.8 Gyrs are shown in Figures 5 and 6, respectively. The plots illustrate the spatial variation of O^+ and $O_2{}^+$, highlighting the evolution of ionospheric ion distribution over time.
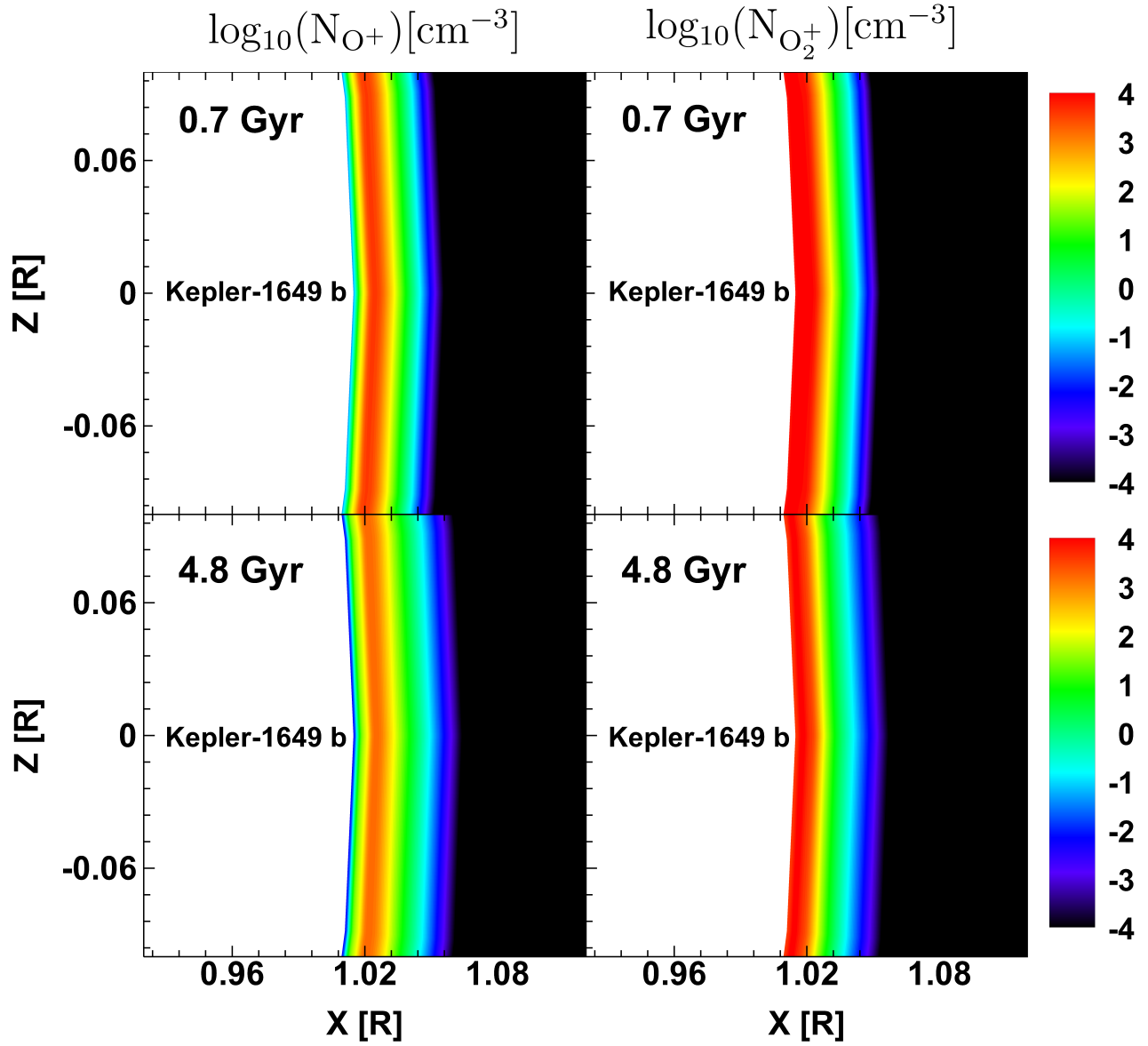
Figure 5. Logarithmic ion number density (cm^{-3}) distributions of O$^+$ (left column) and O$_2^+$ (right column) in the X-Z plane for Kepler-1649 b's dayside at 0.7 Gyr (top row) and 4.8 Gyrs (bottom row). Coordinates are normalized to the planetary radius R_P.
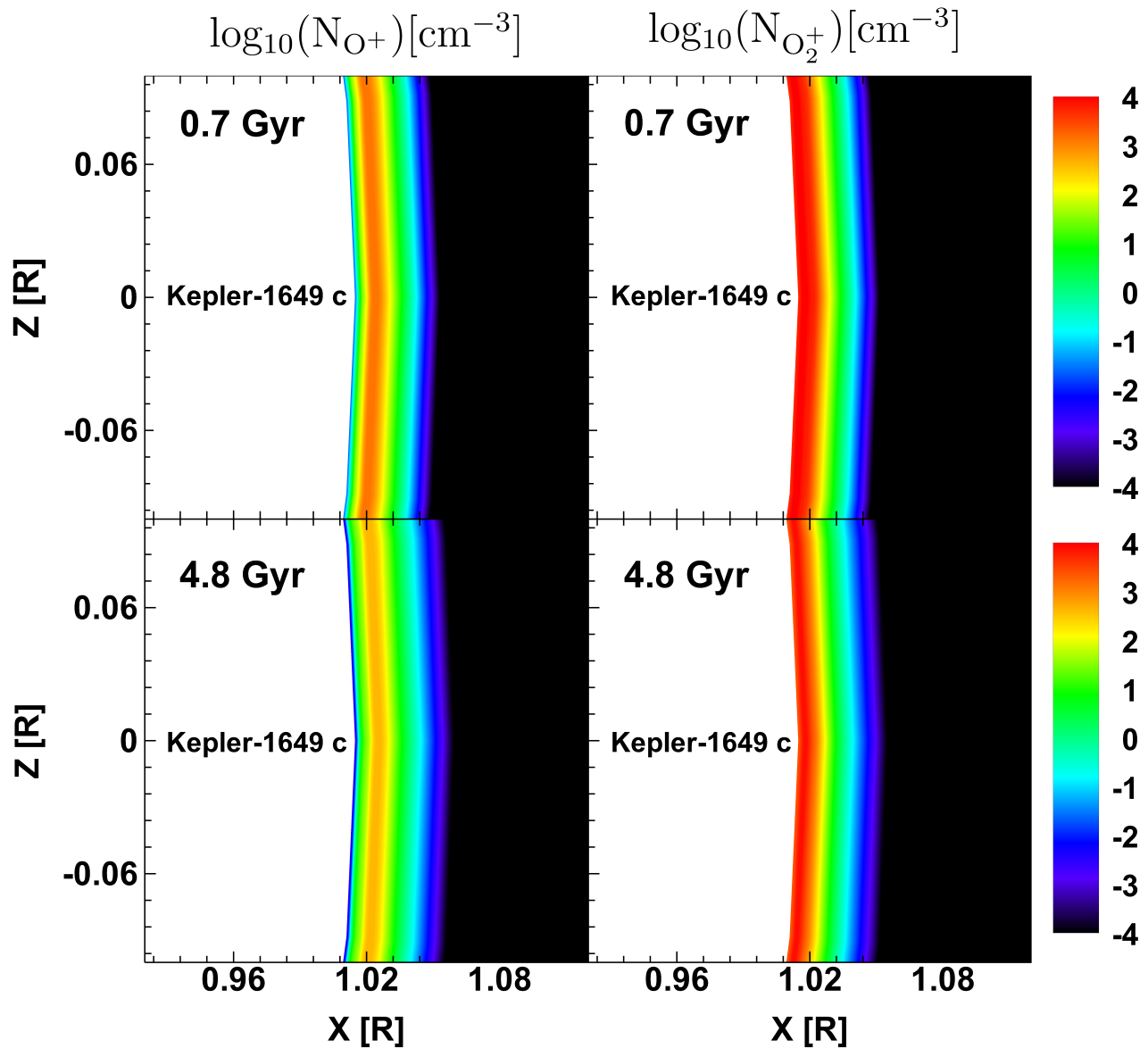
Figure 6. Logarithmic ion number density (cm^{-3}) distributions of O$^+$ (left column) and O$_2{}^+$ (right column) in the X-Z plane for Kepler-1649 c's dayside at 0.7 Gyr (top row) and 4.8 Gyrs (bottom row). Coordinates are normalized to the planetary radius R_{P}.

REFERENCES

Airapetian, V. S., Barnes, R., Cohen, O., et al. 2020, Int. J. Astrobiol., 19, 136, doi: 10.1017/S1473550419000132

Angelo, I., Rowe, J. F., Howell, S. B., et al. 2017, AJ, 153, 162, doi: 10.3847/1538-3881/aa615f

Ballabio, G., & Owen, J. E. 2025, MNRAS, 537, 1305, doi: 10.1093/mnras/staf073

Barstow, M. A., Aigrain, S., Barstow, J. K., et al. 2022, Experimental Astronomy, 54, 1275, doi: 10.1007/s10686-021-09787-9

Bourrier, V., Lovis, C., Beust, H., et al. 2018, Nature, 553, 477, doi: 10.1038/nature24677

Cangi, E., & Chaffin, M. 2024, bluejay: atmospheric photochemistry in Julia, v2.0, Zenodo, doi: 10.5281/zenodo.11307881

Carolan, S., Vidotto, A. A., Hazra, G., Villarreal D'Angelo, C., & Kubyshkina, D. 2021, Monthly Notices of the Royal Astronomical Society, 508, 6001, doi: 10.1093/mnras/stab2947

Catling, D. C., Krissansen-Totton, J., Kiang, N. Y., et al. 2018, Astrobiology, 18, 709, doi: 10.1089/ast.2017.1737

Chin, L., Dong, C., & Lingam, M. 2024, ApJL, 963, L20, doi: 10.3847/2041-8213/ad27d8

Cockell, C. S., Bush, T., Bryce, C., et al. 2016, Astrobiology, 16, 89, doi: 10.1089/ast.2015.1295

Cohen, O., Garraffo, C., Drake, J. J., et al. 2023, The Astrophysical Journal, 949, 54, doi: 10.3847/1538-4357/acc9c2

Cohen, O., Garraffo, C., Moschou, S.-P., et al. 2020, ApJ, 897, 101, doi: 10.3847/1538-4357/ab9637

Coughlin, J. 2020, in American Astronomical Society Meeting Abstracts, Vol. 236, American Astronomical Society Meeting Abstracts #236, 206.08, doi: 10.3847/2041-8213/ab84e5

Dong, C., Huang, Z., & Lingam, M. 2019, ApJL, 882, L16, doi: 10.3847/2041-8213/ab372c

Dong, C., Jin, M., & Lingam, M. 2020, ApJL, 896, L24, doi: 10.3847/2041-8213/ab982f

Dong, C., Jin, M., Lingam, M., et al. 2018, Proceedings of the National Academy of Science, 115, 260, doi: 10.1073/pnas.1708010115

Dong, C., Lingam, M., Ma, Y., & Cohen, O. 2017, ApJL, 837, L26, doi: 10.3847/2041-8213/aa6438

Dong, C., Lee, Y., Ma, Y., et al. 2018, The Astrophysical Journal Letters, 859, L14, doi: 10.3847/2041-8213/aac489

Dotter, A. 2016, ApJS, 222, 8, doi: 10.3847/0067-0049/222/1/8

Engle, S. G. 2024, ApJ, 960, 62, doi: 10.3847/1538-4357/ad0840

Estrela, R., Valio, A., & Palit, S. 2020, in IAU Symposium, Vol. 354, Solar and Stellar Magnetic Fields: Origins and Manifestations, ed. A. Kosovichev, S. Strassmeier, & M. Jardine, 461–466, doi: 10.1017/S1743921320000174

Fox, J. L., & Sung, K. Y. 2001, Journal of Geophysical Research: Space Physics, 106, 21305, doi: https://doi.org/10.1029/2001JA000069

France, K., Loyd, R. O. P., Youngblood, A., et al. 2016, ApJ, 820, 89, doi: 10.3847/0004-637X/820/2/89

France, K., Duvvuri, G., Egan, H., et al. 2020, AJ, 160, 237, doi: 10.3847/1538-3881/abb465

Garcia-Sage, K., Glocer, A., Drake, J. J., Gronoff, G., & Cohen, O. 2017, ApJL, 844, L13, doi: 10.3847/2041-8213/aa7eca

Garraffo, C., Alvarado-Gómez, J. D., Cohen, O., & Drake, J. J. 2022, ApJL, 941, L8, doi: 10.3847/2041-8213/aca487

Garraffo, C., Drake, J. J., & Cohen, O. 2016, ApJL, 833, L4, doi: 10.3847/2041-8205/833/1/L4

Georgakarakos, N. 2003, MNRAS, 345, 340, doi: 10.1046/j.1365-8711.2003.06942.x

—. 2009, MNRAS, 392, 1253, doi: 10.1111/j.1365-2966.2008.14143.x

—. 2013, NewA, 23, 41, doi: 10.1016/j.newast.2013.02.004

Gillet, A., García Muñoz, A., & Strugarek, A. 2023, A&A, 680, A33, doi: 10.1051/0004-6361/202347066

Gonzalez, G. 2005, Origins of Life and Evolution of the Biosphere, 35, 555, doi: 10.1007/s11084-005-5010-8

Grießmeier, J.-M. 2007, Planetary and Space Science, 55, 530, doi: https://doi.org/10.1016/j.pss.2006.11.003

Gronoff, G., Arras, P., Baraka, S., et al. 2020, Journal of Geophysical Research (Space Physics), 125, e27639, doi: 10.1029/2019JA02763910.1002/essoar.10502458.1

Hall, C., Stancil, P. C., Terry, J. P., & Ellison, C. K. 2023, ApJL, 948, L26, doi: 10.3847/2041-8213/acccfb

Harris, C. R., Millman, K. J., van der Walt, S. J., et al. 2020, Nature, 585, 357, doi: 10.1038/s41586-020-2649-2

Hunter, J. D. 2007, Computing in Science and Engineering, 9, doi: 10.1109/MCSE.2007.55

Jakosky, B. M., Brain, D., Chaffin, M., et al. 2018, Icarus, 315, 146, doi: 10.1016/j.icarus.2018.05.030

Kaltenegger, L. 2017, ARA&A, 55, 433, doi: 10.1146/annurev-astro-082214-122238

Kane, S. R., Li, Z., Wolf, E. T., Ostberg, C., & Hill, M. L. 2021, AJ, 161, 31, doi: 10.3847/1538-3881/abcbfd

Kar, A., Henry, T. J., Couperus, A. A., Vrijmoet, E. H., & Jao, W.-C. 2024, AJ, 167, 196, doi: 10.3847/1538-3881/ad2ddc

Khodachenko, M. L., Shaikhislamov, I. F., Lammer, H., et al. 2021, MNRAS, 507, 3626, doi: 10.1093/mnras/stab2366

Kite, E. S., Fegley, Jr., B., Schaefer, L., & Gaidos, E. 2016, ApJ, 828, 80, doi: 10.3847/0004-637X/828/2/80

Krissansen-Totton, J. 2023, ApJL, 951, L39, doi: 10.3847/2041-8213/acdc26

Lammer, H., Kasting, J. F., Chassefière, E., et al. 2008, Space Science Reviews, 139, 399, doi: 10.1007/s11214-008-9413-5

Landin, N. R., Mendes, L. T. S., Vaz, L. P. R., & Alencar, S. H. P. 2023, MNRAS, 519, 5304, doi: 10.1093/mnras/stac3823

Lee, Y., Dong, C., & Tenishev, V. 2021, ApJ, 923, 190, doi: 10.3847/1538-4357/ac26bb

Linsky, J. 2019, Host Stars and their Effects on Exoplanet Atmospheres: An Introductory Overview, Vol. 955 (Springer Cham), doi: 10.1007/978-3-030-11452-7

Luo, J., He, H. Q., Tong, G. S., & Li, J. 2023, ApJ, 951, 136, doi: 10.3847/1538-4357/acd330

Lustig-Yaeger, J., Sotzen, K. S., Stevenson, K. B., et al. 2022, AJ, 163, 140, doi: 10.3847/1538-3881/ac5034

Ma, Y. J., Nagy, A. F., Russell, C. T., et al. 2013, Journal of Geophysical Research (Space Physics), 118, 321, doi: 10.1029/2012JA018265

Madhusudhan, N., Sarkar, S., Constantinou, S., et al. 2023, ApJL, 956, L13, doi: 10.3847/2041-8213/acf577

Modi, A., Estrela, R., & Valio, A. 2023, MNRAS, 525, 5168, doi: 10.1093/mnras/stad2557

Owen, J. E. 2019, Annual Review of Earth and Planetary Sciences, 47, 67, doi: 10.1146/annurev-earth-053018-060246

Owen, J. E., & Mohanty, S. 2016, MNRAS, 459, 4088, doi: 10.1093/mnras/stw959

Parker, E. N. 1958, ApJ, 128, 664, doi: 10.1086/146579

Paxton, B., Bildsten, L., Dotter, A., et al. 2011, ApJS, 192, 3, doi: 10.1088/0067-0049/192/1/3

Peña-Moñino, L., Pérez-Torres, M., Varela, J., & Zarka, P. 2024, A&A, 688, A138, doi: 10.1051/0004-6361/202349042

Popinchalk, M., Faherty, J. K., Kiman, R., et al. 2021, The Astrophysical Journal, 916, 77, doi: 10.3847/1538-4357/ac0444

Priest, E. R. 2012, Solar magnetohydrodynamics, Vol. 21 (Springer Science & Business Media), doi: 10.1007/978-94-009-7958-1

Rackham, B. V., Espinoza, N., Berdyugina, S. V., et al. 2023, RAS Techniques and Instruments, 2, 148, doi: 10.1093/rasti/rzad009

Ribas, I., Gregg, M. D., Boyajian, T. S., & Bolmont, E. 2017, A&A, 603, A58, doi: 10.1051/0004-6361/201730582

Ridgway, R. J., Zamyatina, M., Mayne, N. J., et al. 2023, MNRAS, 518, 2472, doi: 10.1093/mnras/stac3105

Santos, L. A. D., Alam, M. K., Espinoza, N., & Vissapragada, S. 2023, The Astronomical Journal, 165, 244, doi: 10.3847/1538-3881/accf10

Schaefer, L., & Fegley, B. 2007, Icarus, 186, 462, doi: 10.1016/j.icarus.2006.09.002

Schunk, R., & Nagy, A. 2009, Ionospheres: Physics, Plasma Physics, and Chemistry, 2nd edn. (Cambridge: Cambridge Univ. Press)

Schwieterman, E. W., Kiang, N. Y., Parenteau, M. N., et al. 2018, Astrobiology, 18, 663, doi: 10.1089/ast.2017.1729

Seager, S. 2013, Science, 340, 577, doi: 10.1126/science.1232226

See, V., Jardine, M., Vidotto, A. A., et al. 2014, A&A, 570, A99, doi: 10.1051/0004-6361/201424323

Shields, A. L., Ballard, S., & Johnson, J. A. 2016, PhR, 663, 1, doi: 10.1016/j.physrep.2016.10.003

Stevenson, D. J. 2003, Earth and Planetary Science Letters, 208, 1, doi: https://doi.org/10.1016/S0012-821X(02)01126-3

Strangeway, R. J., Ergun, R. E., Su, Y. J., Carlson, C. W., & Elphic, R. C. 2005, Journal of Geophysical Research (Space Physics), 110, A03221, doi: 10.1029/2004JA010829

Teixeira, K. E., Morley, C. V., Foley, B. J., & Unterborn, C. T. 2024, ApJ, 960, 44, doi: 10.3847/1538-4357/ad0cec

Torr, M. R., & Torr, D. G. 1985, J. Geophys. Res., 90, 6675, doi: 10.1029/JA090iA07p06675

Tóth, G., van der Holst, B., Sokolov, I. V., et al. 2012, J. Comp. Phys., 231, 870, doi: 10.1016/j.jcp.2011.02.006

TRAPPIST-1 JWST Community Initiative, de Wit, J., Doyon, R., et al. 2024, Nature Astronomy, 8, 810, doi: 10.1038/s41550-024-02298-5

Tsai, S.-M., Lyons, J. R., Grosheintz, L., et al. 2017, ApJS, 228, 20, doi: 10.3847/1538-4365/228/2/20

Vanderburg, A., Rowden, P., Bryson, S., et al. 2020, ApJL, 893, L27, doi: 10.3847/2041-8213/ab84e5

Varela, J., Brun, A. S., Strugarek, A., et al. 2023, MNRAS, 525, 4008, doi: 10.1093/mnras/stad2519

Virtanen, P., Gommers, R., Oliphant, T. E., et al. 2020, Nature Methods, 17, 261, doi: 10.1038/s41592-019-0686-2

Wood, B. E., Müller, H. R., Zank, G. P., Linsky, J. L., & Redfield, S. 2005, ApJL, 628, L143, doi: 10.1086/432716

Wordsworth, R., & Kreidberg, L. 2022, ARA&A, 60, 159, doi: 10.1146/annurev-astro-052920-125632

Yang, J., & Hu, R. 2024, ApJ, 966, 189, doi: 10.3847/1538-4357/ad35c8

Zendejas, J., Segura, A., & Raga, A. C. 2010, Icarus, 210, 539, doi: 10.1016/j.icarus.2010.07.013

Zhu, W., & Dong, S. 2021, ARA&A, 59, 291, doi: 10.1146/annurev-astro-112420-020055